ADVANCED FUNCTIONAL MATERIALS
www.afm-journal.de

www.MaterialsViews.com

High-Speed and Low-Energy Nitride Memristors

Byung Joon Choi, Antonio C. Torrezan, John Paul Strachan, P. G. Kotula, A. J. Lohn, Matthew J. Marinella, Zhiyong Li, R. Stanley Williams, and J. Joshua Yang**

High-performance memristors based on AlN films have been demonstrated, which exhibit ultrafast ON/OFF switching times (≈85 ps for microdevices with waveguide) and relatively low switching current (≈15 µA for 50 nm devices). Physical characterizations are carried out to understand the device switching mechanism, and rationalize speed and energy performance. The formation of an Al-rich conduction channel through the AlN layer is revealed. The motion of positively charged nitrogen vacancies is likely responsible for the observed switching.

1. Introduction

Rapidly growing smart mobile platforms and their electronic infrastructure will require high-performance and low-energy nonvolatile memories to realize the potential of the Internet of Things (IoT).[1–3] Oxide based memristors or resistance random access memories (RRAM) have been strong candidates among the emerging nonvolatile memories.[4–13] Non-oxide switching materials, however, represent an even larger and yet little explored material pool that can potentially offer more desirable device properties, including high-speed and low-energy switching.[14–22] In addition, a nitride switching material would have a better process and chemical compatibility with nitride (e.g., TiN and TaN) electrodes,[13,14,23] which are generally used in CMOS fabs for commercial circuits. Furthermore, nitride memristors may be readily extended to power electronic devices, where nitride compound semiconductors, such as GaN, $Al_xGa_{1-x}N$, and $In_xGa_{1-x}N$, are used as channel materials for high electron mobility transistors (HEMT)[24,25] that can provide the high speeds and voltages required to drive ultrafast memristors. More importantly, since these nitride compound semiconductors can also serve as memristive switching materials, the integration process of nitride memristors onto HEMTs is straightforward, i.e., adding a layer of electrode onto the existing nitride materials.[25]

We have previously demonstrated that AlN-based memristors exhibited reversible and reproducible memristive switching characteristics with various electrode materials, such as Pt, TiN, and Al.[14] In this study, we first demonstrate ultrahigh switching speed (85 ps), low switching current (sub 15 µA) and scalability to the nanoscale for the nitride memristors, and then imaging of the switching channels to better understand the switching mechanism of these devices

2. Results and Discussion

Using nanoimprint lithography and lift-off processes, we have fabricated 50 nm × 50 nm nitride memristors and observed low switching currents, as shown in **Figure 1**a and its inset. Figure 1b shows typical quasi-DC switching *I*–*V* loops of a TiN (15 nm)/AlN (6 nm)/Pt (15 nm) device. A pristine nitride device was highly resistive, as expected for a wide band gap AlN film. Initially, the device was electroformed to its on-state by a positive bias sweep on the TiN electrode. A current compliance of 10 µA was set for the electroforming process. Then, an opposite polarity DC sweep switched it back to the off-state. Both the on- and off-switching currents were below 15 µA, which is about an order of magnitude lower than that of a comparable $Pt/TiO_2/Pt$ oxide fabricated by the same procedure and with the same size, as shown in Figure S1 of the Supporting Information.

An AlN memristor switched both off and on in 85 ps, which is the fastest among all resistance switches reported so far. The high series resistance of the electrode (a few kΩ) of the lab-fabricated nanodevices prevented us from delivering sub-ns electrical pulses to these memristors. Therefore, a specifically designed and fabricated structure with transmission lines was used for the high speed measurements.[8] A 5 µm × 5 µm memristor with a TiN (20 nm)/AlN (6 nm)/Pt (60 nm) stack was set to its on-state after electroforming using the DC sweep mode (see Figure S2, Supporting Information). For microdevices, 0.1 to a few mA level of compliance current was required for

Prof. B. J. Choi, Dr. A. C. Torrezan, Dr. J. P. Strachan, Dr. Z. Li, Dr. R. S. Williams, Prof. J. J. Yang
Hewlett Packard Labs
Palo Alto, CA 94304, USA
E-mail: stan.williams@hpe.com; jjyang@umass.edu
Prof. B. J. Choi
Department of Materials Science and Engineering
Seoul National University of Science and Technology
Seoul 01811, South Korea
Dr. P. G. Kotula, Dr. A. J. Lohn, Dr. M. J. Marinella
Sandia National Laboratories
Albuquerque, NM 87185, USA
Prof. J. J. Yang
Department of Electrical and Computer Engineering
University of Massachusetts
Amherst, MA 01003, USA

DOI: 10.1002/adfm.201600680

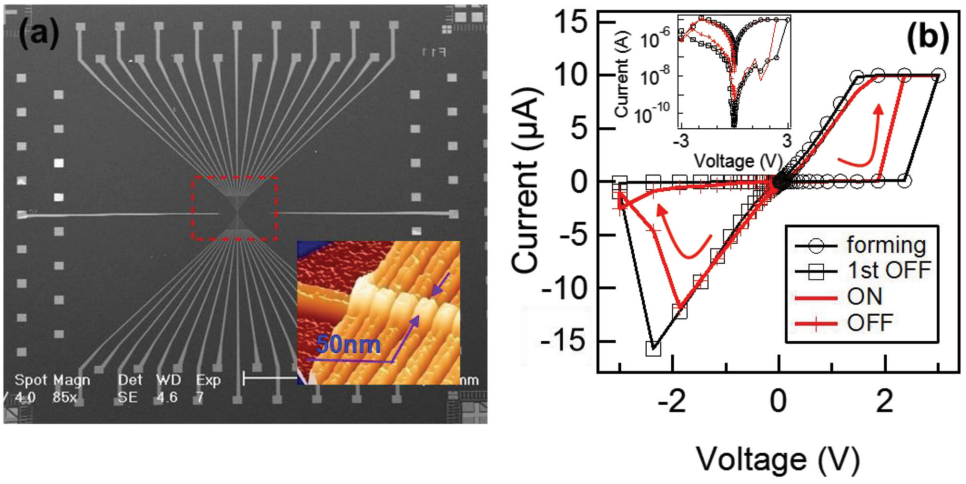

Figure 1. Nanoscale memristors with low switching current. a) Scanning electron microscopy image of a 1 × 17 memristor array with a material stack of TiN (15 nm)/AlN (6 nm)/Pt (15 nm). The inset shows the atomic force microscopy image of the 50 nm × 50 nm memristors. b) Typical quasi-DC switching *I*–*V* loops of a nanodevice, showing both the electroforming and subsequent switching loops. The inset presents the same data in a semi-log scale plot.

the electroforming process. **Figure 2**a reveals the off-switching when a −1.9 V pulse with a full width at half maximum (FWHM) of ≈85 ps was applied to the TiN electrode. The large resistance change from 0.73 to 97.83 kΩ was confirmed by a subsequent read pulse. The results from two attempts using pulses with the same FWHM but smaller voltage amplitudes are also shown in Figure 2a, and reveal that the device was not (or not fully) switched off by those smaller pulses. After that, the resistance state could be successfully set to 0.73 kΩ by applying an opposite polarity (positive) voltage pulse with the same pulse-width. Figure 2b shows the dramatic change of the on-switching current with increasing voltage pulse amplitudes (from +0.8 to +2.1 V). We have observed about 100 ps switching time with oxide switching materials (e.g., TaO_x and SiO_2), with a similar high current recorded in the ultrafast time domain.[8,26] The high switching current in the fast operation mode results from the strong nonlinearity of the current–voltage characteristic coupled with the two order of magnitude decrease in base resistance of the device. An Arrhenius-type relationship between the ionic motion and electric field[27] or the exponential dependence of mobility on electric field[28] might be a major reason for such a highly nonlinear voltage–time dependency, i.e., ultrafast switching speed.

A Pt–free nitride memristor with the material stack of Al/AlN/TiN is presented in **Figure 3**a, and exhibits a similar pinched-hysteresis loop as that of the Al/AlN/Pt device shown in Figure 3b. Technologically, it is important to replace noble metal electrodes used in research devices by metal nitride electrodes for commercialization, because of the high cost and the difficulties in etching processes associated with noble metals. Scientifically, the observed independence of the *I*–*V* characteristics on Pt or TiN electrodes means that the physical properties of the electrode materials and interface contacts, such as work functions and Schottky barriers, do not substantially affect the resistance change during switching. Furthermore, this insensitivity of the switching behavior to the electrode material can reduce the practical challenges of device reproducibility caused by complex interface reactions and contamination in the fabrication processes. However, the switching polarity does depend on the chemical properties, especially the N accommodation capability of the electrode materials. Both Al and TiN electrodes can accommodate nitrogen and thus serve as N reservoirs, which play a similar role as the Ta electrode in a Ta/TaO_x/Pt device.[23,29] The switching polarity of the Al/AlN/TiN device in Figure 3a suggests that the AlN/TiN interface is the switching interface, which is normally observed for the more chemically inert interface, such as the AlN/Pt interface in Figure 3b. The Al/AlN top interface is expected to be electrically more conductive due to the existence of a large concentration of N vacancies.[30,31]

To understand the switching mechanism for the AlN switching material, we compare it to the more intensively studied TaO_x system because of the similarities in their phase diagrams and switching behavior (e.g., linear *I*–*V* curves in the ON and OFF states as shown in Figure S3, Supporting Information). The linear *I*–*V* curves in both the ON and the OFF states in TaO_x devices indicate that a conducting channel bridges the two electrodes both in the ON state and the OFF states. The resistance change of TaO_x is mainly caused by modulating the chemical composition of the conducting channel, rather than modulating a tunneling gap between the tip of the channel and an electrode as observed in TiO_x systems.[13,29,32,33] The TaO_x conducting channel is composed of a Ta(O) solid solution (Ta with dissolved O), which was confirmed by pressure-modulated conductance microscopy (PMCM)[33,34] and focused ion beam- transmission electron microscopy (FIB-TEM).[29] Similarly, in the Al-N system, there are only two thermodynamically stable solid phases, i.e., the insulating AlN and metallic Al phases. Considering that the *I*–*V* curves of both the ON and the OFF states are also fairly linear for the AlN microdevices, we expect a similar switching mechanism for the AlN microdevice, i.e., the composition modulation of an Al-rich conducting channel. The composition modulation is realized by the drift of mobile species in the applied electric field, which could be assisted by thermal processes caused by Joule heating. The

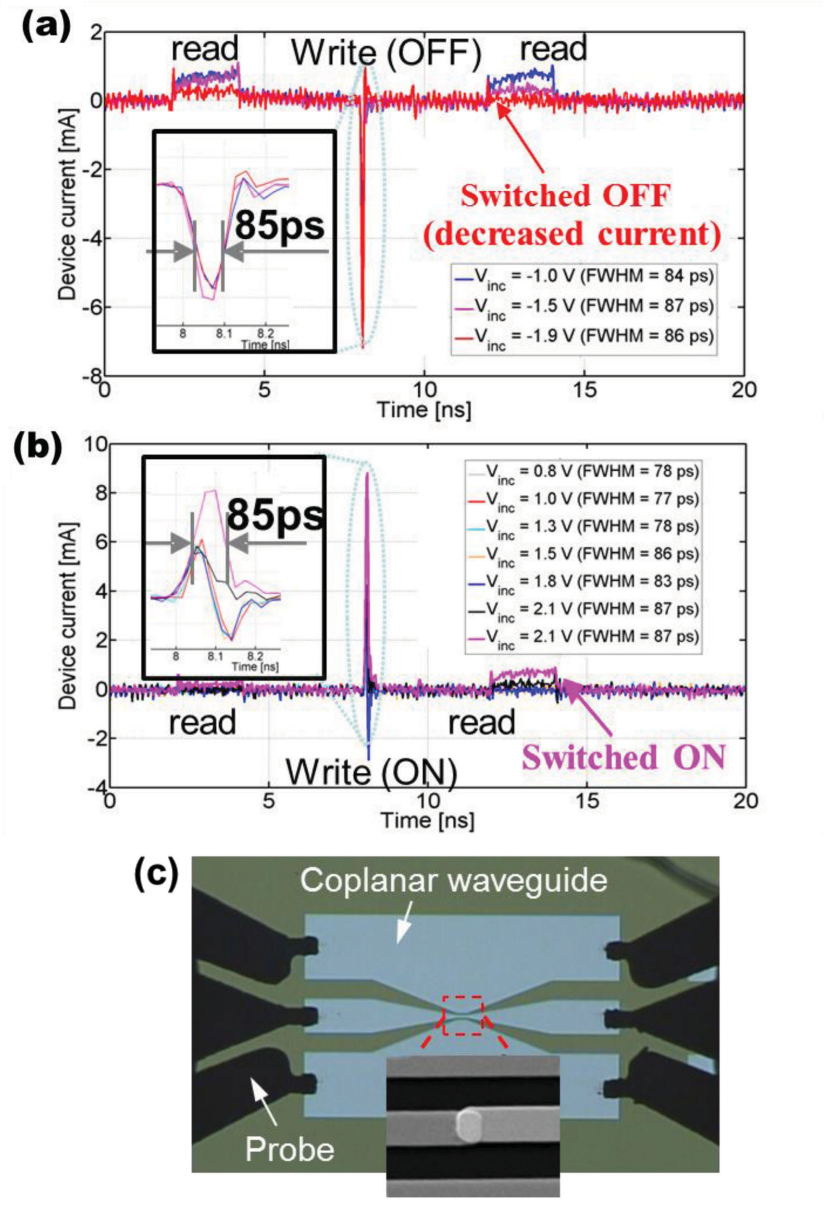

Figure 2. Ultrafast switching of the AlN memristor. a) OFF switching using an 85 ps voltage pulse and b) ON switching using an 85 ps voltage pulse. The insets to (a) and (b) give the zoom-in image of the switching pulses. Before and after the switching pulse, a read pulse was applied to verify the device resistance state. In both ON and OFF switching, three attempts with an increasing voltage magnitude were used. The devices were successfully switched when the voltage reached the threshold voltage, i.e., –1.9 V for OFF switching (red curve in (a)) and +2.1 V for ON switching (purple curve in (b)). c) The optical microscopy image of the measurement setup. The inset shows the scanning electron microscopy image of the device used for the high speed measurements.

linear ON state *I*–*V* curve and nonlinear OFF state *I*–*V* curve of the nanodevices suggest that electronic barriers form during the OFF switching in nanodevices to rupture the metallic conduction channel of the ON state.[35] The low switching currents observed in nanodevices combined with the very high AlN thermal conductivity (>10 × higher than TaO_x) may indicate a minimized role of Joule heating in the switching of nanoscale devices.

To image the conduction channel, cross-sectional scanning transmission electron microscopy (STEM) combined with chemical analysis (energy dispersive spectroscopy and electron energy loss spectroscopy) were performed. Here the same Al/AlN/Pt device from Figure 3b was used, which was fabricated by means of a shadow mask (≈100 µm diameter) to eliminate the incorporation of moisture and organic resist during wet processing in the usual fabrication process. A Pt film was deposited over the Al top electrode (TE) without breaking the vacuum to minimize Al oxidation. The as-fabricated device was then electroformed (positive bias applied to the Al TE), switched a few times by using the quasi-DC sweeping mode and then left in the ON state, which resulted in a morphological change inside the device area indicated by an arrow in **Figure 4**a (left). Pressure modulated conducting microscopy (PMCM)[34] was used to confirm that the morphological change was spatially coincident with the location of the conduction channel, as indicated by the green arrow in the PMCM image of Figure 4a (right). Here the dark spot represents an electrically conducting region, i.e., a conduction channel or the switching region. Cross-sectioning this region (①, referred to as switching region) together with a neighboring region (②, referred to as intact region, for comparison) was performed by FIB milling to obtain a STEM sample.

The top contact Pt/Al electrode was considerably deformed in the switching region compared with the intact region, as can be seen from Figure S4a,b of the Supporting Information. Some of the Al diffused through the Pt film and was oxidized, indicating that this active region experienced significant Joule heating, and possibly ionic motion during the electroforming and perhaps the switching operations as well. Electron energy loss spectroscopy (EELS) of the nitrogen *K*-edge revealed a substantial N deficiency in the top part (next to the Al layer) of the AlN film in the switching region, as can be seen by comparing Figure 4c,d. Whereas, the nitrogen deficiency seems to be compensated by the increase of oxygen concentration in the top part of the AlN film, which is revealed by the EELS of the oxygen *K*-edge as shown in Figure 4f. Figure 4e suggests that the surface of the AlN film in the intact region already contains a small amount of oxygen. This originated from a brief exposure to air while transferring the AlN film from an ALD chamber to an evaporation chamber for the top electrode layer deposition. The oxygen level in our ALD-grown AlN films is below 1%, much lower than that in typical PVD- or CVD-grown AlN films.[14,36,37] The larger oxygen signal found in

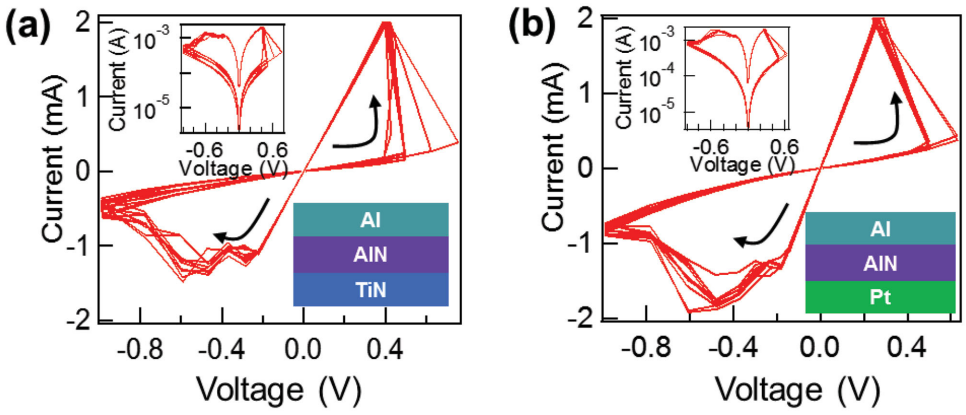

Figure 3. Comparison of two memristors with different material stacks and similar switching characteristics, including switching polarity and voltages. The insets present the same data in a semi-log plot.

the active switching region of the operated device is likely the result of oxygen from the atmosphere diffusing into the device during electrical operation. These EELS results suggest that a significant amount of the upper AlN layer was turned into an oxynitride (AlO_xN_y) during electrical operation due to the intermixing of nitrogen in AlN and oxygen in the top interfacial layer.[38] However, the bottom AlN/Pt(BE) interface remained relatively clean, since the oxygen level was as low as that in the bottom Pt film (see Figure S5, Supporting Information).

The above results have shown that the films in the pristine state are relatively oxygen free and remain so in most of the device volume even after electrical operation. However, the

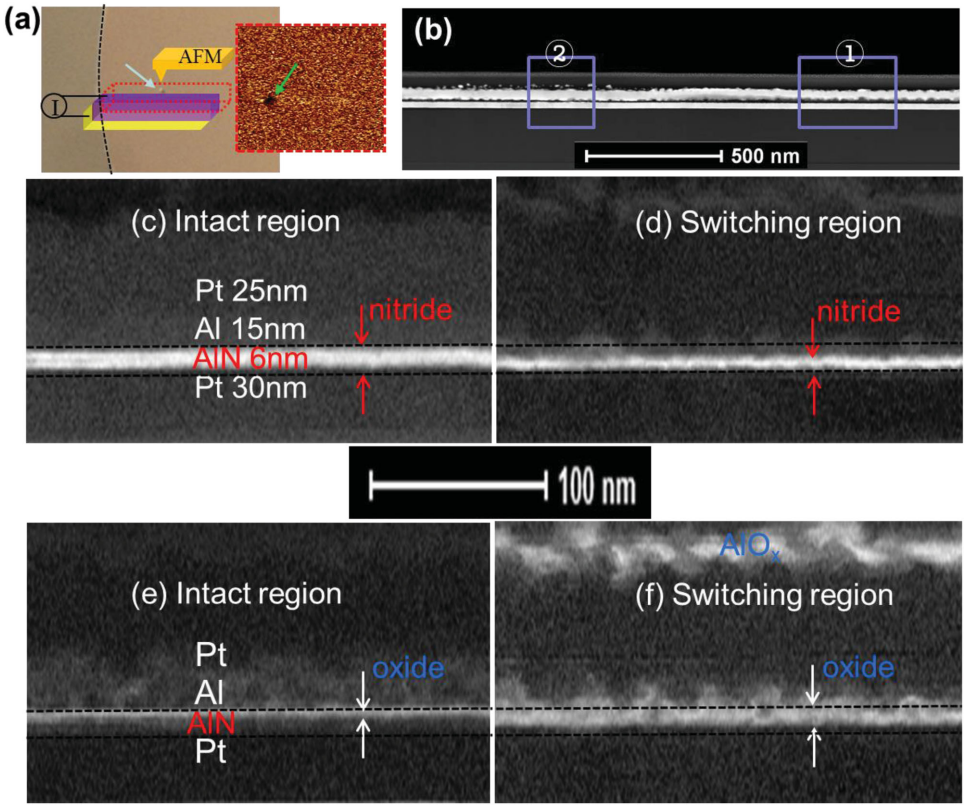

Figure 4. Visualization of the conduction channel of the nitride memristor. a) The main micrograph (light brown) is an optical image of a part of a disk device after electrical operations, showing a small bubble-like morphology change indicated by a blue arrow. The dashed line is the boundary of the disk (top electrode). The cartoon (left) schematically shows the pressure-modulated conductance microscopy (PMCM). The PMCM image (right) around the bubble region reveals a conduction channel indicated by a green arrow. b) Cross-section transmission electron microscopy micrograph across the conduction channel as well as some intact region. c,d) Electron energy loss spectroscopy (EELS) maps of *K*-edge of nitrogen for the intact and switching regions, respectively. e,f) Electron energy loss spectroscopy (EELS) maps of *K*-edge of oxygen for the intact and switching regions, respectively.

localized switching region may be contaminated by oxygen from the device operation environment, which can only be observed by careful examination. Therefore, the role of oxygen impurities in the nitride film needs to be discussed.[39–43] Oxygen incorporation into an AlN film is expected, since the bond dissociation energy of Al–O (481 ± 21 kJ mol^{-1} at 0 K) is much higher than that of Al-N (297 kJ mol^{-1} at 0 K) or Al–Al (188 ± 42 kJ mol^{-1} at 0 K).[44,45] Based on the calculated formation energy of a point defect, substitutional O_N should be a very energetically favorable defect in AlN, in agreement with the experimental observation of easy contamination of AlN by oxygen.[39] However, a high oxygen concentration does not lead to an enhanced electrical conduction, since the deep energy levels of neutral O_N or positively charged O_N^+ in AlN can neither serve as mobile charge carriers nor contribute to a lower activation energy for electrical conductivity.[39,42,43] Rather than a contribution to electrical conduction, one can expect that incorporated oxygen replaces nitrogen and thus provides additional mobile nitrogen ions, which may enhance ionic motion and ultimately formation of nitrogen bubbles.

An EELS composition mapping of the intact region is presented in **Figure 5**a. AlN (red) and AlO_x (blue) layers are clearly differentiated. Figure 5b shows a composition mapping of a cross-section of the switching region, where the metallic Al (green) layer has completely disappeared and two AlOx layers have appeared on both side of the Pt layer (also shown in Figure 4d,f). In addition, the AlN (red) layer was partially inter mixed with the AlO_x (blue) layer next to it (Figure 5b, magenta = red plus blue). There is a peculiarly thin region in the AlN layer, which is indicated in a box with red dashed lines in Figure 5b and seems to be Al-rich with greenish clusters, i.e., metallic Al. The thin and Al-rich regions are likely the conduction channels of the device. Based on the electrical measurements, TEM observations, and the possible point defects involved, a plausible switching mechanism is proposed in Figure 5c,d. The AlN/Pt interface is assigned to be the active switching interface, and the motion of nitrogen vacancies (V_N^{3+}) is responsible for the switching. Aluminum interstitial (Al_i^{3+}) is another possible candidate as the mobile species here. However, it is more likely that most of the aluminum interstitials are swept into the interfaces with the Pt electrodes by image forces and stuck at the interface regions. Nitrogen deficiency can be generated when the Al top contact steals some N from the AlN layer. Electroforming may enhance this reaction or even strip N atoms from the AlN layer by forming N_2 bubbles.[46] Experimentally, we observed swollen regions on the top electrode (Figure S6,

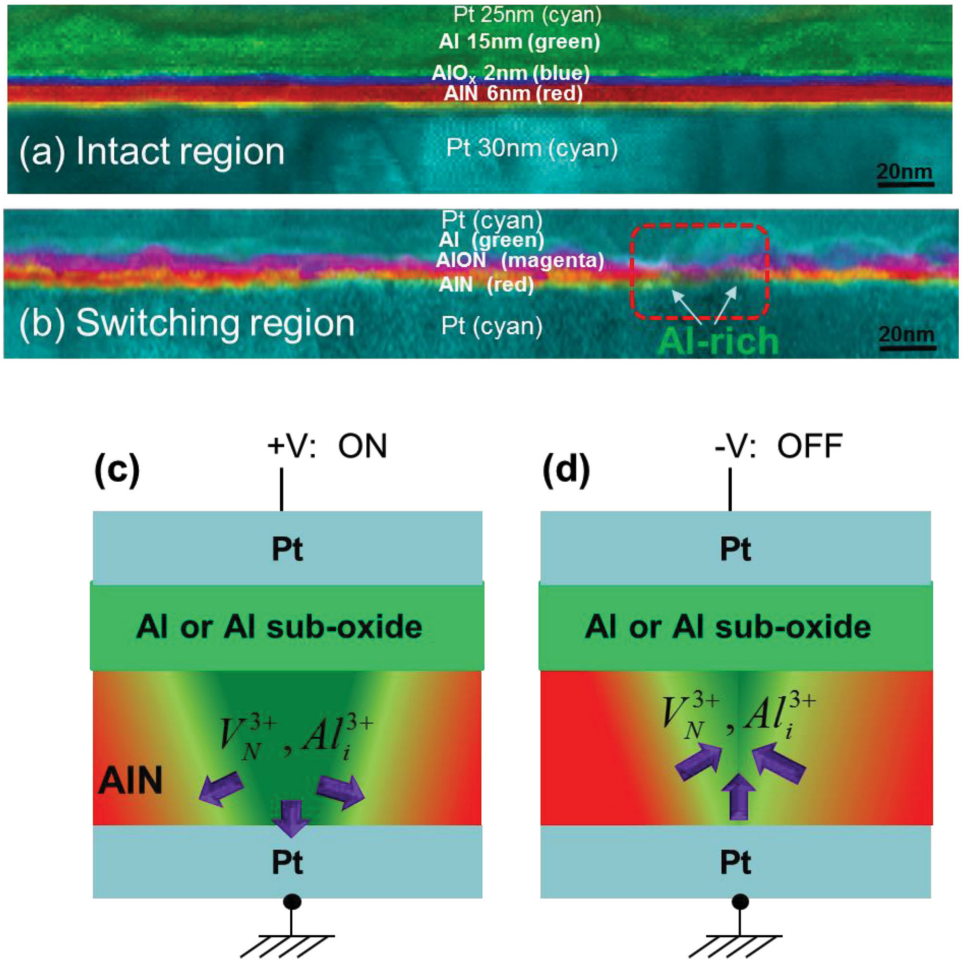

Figure 5. Switching mechanism of the nitride memristor. a,b) Cross-sectional STEM-EELS compositional images for (a) the intact region and (b) the switching region. c,d) Schematics illustrating the ON and OFF switchings, respectively.

Supporting Information). The calculated formation energy of V_N^{3+} for Al-rich conditions (2.7 eV) is much lower than that for N-rich conditions (6.6 eV).[42] Accordingly, a higher V_N^{3+} concentration is expected in Al-rich conduction channels. The diffusivity of V_N^{3+} can be estimated from Frenkel theory,[28,47,48] but the jump attempt frequency and activation energy for these species in AlN are not available. The large charge number of V_N^{3+} results in a larger force on the vacancy for the same applied field, which could lead to a much larger drift velocity since the drift can be strongly nonlinear. It is worth noting that we could not completely exclude the possibility that oxygen anion or oxygen vacancies serves as mobile species during the switching based on the experimental results.

We did not identify an Al-rich conduction channel from an AlN matrix (see Figures S7,S8, Supporting Information) by using scanning transmission X-ray microscopy (STXM, resolution ≈30 nm). It is likely that the extraction of nitrogen may induce a local excess of Al without altering the chemical bonding state of AlN, which may lead to the formation of Al-rich conduction channels with low dimensionality (lower than the STXM resolution). The low dimensionality is possibly related to the solubility of mobile species in the conduction channels. In contrast to TaO_x memristors, where the Ta(O) channel has a large solubility of O and can thus accommodate a large amount of O to form a sizable channel, the Al-rich channel has a very limited N solubility and thus a smaller size. Both the small channel size and the relatively low melting temperature of Al metal (660 °C) may have contributed to the ultrafast switching and low energy consumption in the nitride device, in contrast to the high melting temperature of Ta (3020 °C) or Ti (1668 °C) in the oxide systems. A high diffusivity of Al cations and reactivity with nitrogen in conduction channels near the melting temperature may accelerate the ion motion in the conduction channels.[49]

3. Conclusions

In summary, we measured an ultrafast switching time of 85 ps in AlN memristors and an order of magnitude lower switching current than that of comparable nanoscale oxide devices. Switching occurred mainly at the more inert metal/nitride interface of the device, such as the TiN/AlN interface in a TiN/AlN/Al memristor. As observed using STEM-EELS analysis, the top interface of AlN (e.g., the AlN/Al interface) was oxidized to result in an AlO_xN_y phase above the active switching region, which is expected to be typical for all nitride memristors due to the thermodynamically favorable formation of O_N defects in nitrides. Evolution of the oxynitride phase is believed to facilitate the formation of the Al-rich conduction channel at the switching interface, where the motion of V_N^{3+} and/or Al_i^{3+} is likely responsible for the observed switching.

4. Experimental Section

Device Fabrication: Devices were fabricated with a wide range of junction area from 0.0025 to 31 450 μm^2. E-beam evaporated Pt/Al or sputter-grown TiN metal lines were used as bottom electrode, which was patterned by shadow mask or photolithography for microscale device and nanoimprint lithography was used for nanoscale device. AlN thin films were deposited by remote plasma enhanced atomic layer deposition (ALD) using Trimethylaluminum (TMA, $Al(CH_3)_3$) and N_2:H_2 (20:40 SCCM) mixed gas as a metal organic precursor and a reactant gas at a wafer temperature of 350 °C. For the cross-point device, a Pt/Al top electrode was deposited by electron-beam evaporation either through a shadow mask or lithographically patterned forming cross-point junction device.

Characterization: the four-terminal *I–V* characteristics of the devices were measured using a semiconductor parameter analyzer (HP-4156). A quasi-DC voltage sweep (sweep rate from 10^0 to 10^2 V s^{-1}) was applied to the top electrode with the bottom contact grounded at ambient temperature in all the electrical measurements. In order to explore fast switching speeds in these films, device was integrated with a coplanar waveguide, which enables sub-ns voltage pulses to be introduced to the device and the switching to be monitored in real time with 25 ps resolution using a Lecroy 820Zi-A. Series resistance and parasitic capacitance of the device were determined from measured frequency and time responses of virgin devices and verified by circuit modeling (see Figure S2b, Supporting Information). Details of the setup and device geometry can be found in previous work.[8,26]

Supporting Information

Supporting Information is available from the Wiley Online Library or from the author.

Acknowledgements

B.J.C. was supported by Basic Science Research Program through the National Research Foundation of Korea (NRF) funded by the Ministry of Education (2014R1A1A2054597). Sandia is a multiprogram laboratory operated by Sandia Corporation, a Lockheed Martin Company, for the United Stated Department of Energy (DOE) under Contract No. DEAC0494AL85000.

Received: February 5, 2016
Revised: March 24, 2016
Published online: May 24, 2016

[1] R. F. Freitas, W. W. Wilcke, *IBM J. Res. Dev.* **2008**, *52*, 439.
[2] S. Borkar, *Proc. Symp. VLSI-DAT*, IEEE, **2010**, 2.
[3] L. Van Den Hove, *IEDM Tech. Dig.* **2012**, 12.
[4] Y. Naruke, S. Mori, N. Hayasaka, T. Process, T. Liu, *Int. Solid-State Circuits Conf. (ISSCC)* **2013**, 210.
[5] Y. Y. Chen, R. Degraeve, S. Clima, B. Govoreanu, L. Goux, A. Fantini, G. S. Kar, G. Pourtois, G. Groeseneken, D. J. Wouters, M. Jurczak, *IEDM Tech. Dig.* **2012**, 10.
[6] B. Govoreanu, G. S. Kar, Y. Chen, V. Paraschiv, S. Kubicek, A. Fantini, I. P. Radu, L. Goux, S. Clima, R. Degraeve, N. Jossart, O. Richard, T. Vandeweyer, K. Seo, P. Hendrickx, G. Pourtois, H. Bender, L. Altimime, D. J. Wouters, J. A. Kittl, M. Jurczak, B. Leuven, K. U. Leuven, *IEDM Tech. Dig.* **2011**, 729.
[7] M.-J. Lee, C. B. Lee, D. Lee, S. R. Lee, M. Chang, J. H. Hur, Y. Kim, C. Kim, D. H. Seo, S. Seo, U. Chung, I. Yoo, K. Kim, *Nat. Mater.* **2011**, *10*, 625.
[8] A. C. Torrezan, J. P. Strachan, G. Medeiros-Ribeiro, R. S. Williams, *Nanotechnology* **2011**, *22*, 485203.

[9] J. J. Yang, M. D. Pickett, X. Li, D. A. A. Ohlberg, D. R. Stewart, R. S. Williams, *Nat. Nanotechnol.* **2008**, *3*, 429.
[10] R. Waser, M. Aono, *Nat. Mater.* **2007**, *6*, 833.
[11] B. J. Choi, D. S. Jeong, S. K. Kim, C. Rohde, S. Choi, J. H. Oh, H. J. Kim, C. S. Hwang, K. Szot, R. Waser, B. Reichenberg, S. Tiedke, *J. Appl. Phys.* **2005**, *98*, 033715.
[12] S. Seo, M. J. Lee, D. H. Seo, E. J. Jeoung, D.-S. Suh, Y. S. Joung, I. K. Yoo, I. R. Hwang, S. H. Kim, I. S. Byun, J.-S. Kim, J. S. Choi, B. H. Park, *Appl. Phys. Lett.* **2004**, *85*, 5655.
[13] J. J. Yang, D. B. Strukov, D. R. Stewart, *Nat. Nanotechnol.* **2013**, *8*, 13.
[14] B. J. Choi, J. J. Yang, M.-X. Zhang, K. J. Norris, D. A. A. Ohlberg, N. P. Kobayashi, G. Medeiros-Ribeiro, R. S. Williams, *Appl. Phys. A* **2012**, *109*, 1.
[15] H.-D. Kim, H.-M. An, E. B. Lee, T. G. Kim, *IEEE Trans. Electron Devices* **2011**, *58*, 3566.
[16] Q. Lu, X. Zhang, W. Zhu, Y. Zhou, Q. Zhou, L. Liu, X. Wu, *Phys. Status Solidi* **2011**, *208*, 874.
[17] H.-D. Kim, H.-M. An, T. G. Kim, *J. Appl. Phys.* **2011**, *109*, 016105.
[18] D.-I. Kim, J. Yoon, J.-B. Park, H. Hwang, Y. M. Kim, S. H. Kwon, K. H. Kim, *Appl. Phys. Lett.* **2011**, *98*, 152107.
[19] C. Chen, Y. C. Yang, F. Zeng, F. Pan, *Appl. Phys. Lett.* **2010**, *97*, 083502.
[20] H.-D. Kim, H.-M. An, K. C. Kim, Y. Seo, K.-H. Nam, H.-B. Chung, E. B. Lee, T. G. Kim, *Semicond. Sci. Technol.* **2010**, *25*, 065002.
[21] M. J. Yun, H.-D. Kim, S. Man Hong, J. Hyun Park, D. Su Jeon, T. Geun Kim, *J. Appl. Phys.* **2014**, *115*, 094305.
[22] C. Chen, S. Gao, G. Tang, H. Fu, G. Wang, C. Song, F. Zeng, F. Pan, *ACS Appl. Mater. Interfaces* **2013**, *5*, 1793.
[23] J. J. Yang, M.-X. Zhang, J. P. Strachan, F. Miao, M. D. Pickett, R. D. Kelley, G. Medeiros-Ribeiro, R. S. Williams, *Appl. Phys. Lett.* **2010**, *97*, 232102.
[24] U. K. Mishra, P. Parikh, *Proc. IEEE* **2002**, *90*, 1022.
[25] J. W. Chung, W. E. Hoke, E. M. Chumbes, T. Palacios, *IEEE Electron Device Lett.* **2010**, *31*, 195.
[26] B. J. Choi, A. C. Torrezan, K. J. Norris, F. Miao, J. P. Strachan, M.-X. Zhang, D. A. A. Ohlberg, N. P. Kobayashi, J. J. Yang, R. S. Williams, *Nano Lett.* **2013**, *13*, 3213.
[27] S. Menzel, M. Waters, A. Marchewka, U. Böttger, R. Dittmann, R. Waser, *Adv. Funct. Mater.* **2011**, *21*, 4487.
[28] D. B. Strukov, R. S. Williams, *Appl. Phys. A* **2009**, *94*, 515.
[29] F. Miao, J. P. Strachan, J. J. Yang, M.-X. Zhang, I. Goldfarb, A. C. Torrezan, P. Eschbach, R. D. Kelley, G. Medeiros-Ribeiro, R. S. Williams, *Adv. Mater.* **2011**, *23*, 5633.
[30] F. A. Chudnovskii, L. L. Odynets, A. L. Pergament, G. B. Stefanovich, *J. Solid State Chem.* **1996**, *122*, 95.
[31] D. S. Jeong, R. Thomas, R. S. Katiyar, J. F. Scott, H. Kohlstedt, A. Petraru, C. S. Hwang, *Rep. Prog. Phys.* **2012**, *75*, 076502.
[32] J. P. Strachan, M. D. Pickett, J. J. Yang, S. Aloni, D. A. L. Kilcoyne, G. Medeiros-Ribeiro, R. S. Williams, *Adv. Mater.* **2010**, *22*, 3573.
[33] F. Miao, J. J. Yang, J. P. Strachan, D. Stewart, R. S. Williams, C. N. Lau, *Appl. Phys. Lett.* **2009**, *95*, 113503.
[34] C. N. Lau, D. R. Stewart, R. S. Williams, M. Bockrath, *Nano Lett.* **2004**, *4*, 569.
[35] A. Marchewka, B. Roesgen, K. Skaja, H. Du, C.-L. Jia, J. Mayer, V. Rana, R. Waser, S. Menzel, *Adv. Electron. Mater.* **2016**, *2*, 1500233.
[36] M. Alevli, C. Ozgit, I. Donmez, N. Biyikli, *Phys. Status Solidi* **2012**, *209*, 266.
[37] C. Ozgit, I. Donmez, M. Alevli, N. Biyikli, *Thin Solid Films* **2012**, *520*, 2750.
[38] M. J. Marinella, J. E. Stevens, E. M. Longoria, P. G. Kotula, *70th Device Research Conf.*, IEEE, **2012**, 89.
[39] T. Mattila, R. Nieminen, *Phys. Rev. B: Condens. Matter* **1996**, *54*, 16676.
[40] C. G. Van de Walle, C. Stampfl, J. Neugebauer, *J. Cryst. Growth* **1998**, *189*, 505.
[41] V. Serin, C. Colliex, R. Brydson, S. Matar, F. Boucher, *Phys. Rev. B* **1998**, *58*, 5106.
[42] I. Gorczyca, A. Svane, N. Christensen, *Phys. Rev. B* **1999**, *60*, 8147.
[43] C. Stampfl, C. Van de Walle, *Phys. Rev. B* **2002**, *65*, 155212.
[44] B. De, B. Darwent, *Nat. Stand. Ref. Data Ser.* **1970**, 1.
[45] J. A. Dean, *Handbook of Chemistry*, 5th ed., McGraw-Hill, Inc, New York, NY, USA **1999**.
[46] J. J. Yang, F. Miao, M. D. Pickett, D. A. A. Ohlberg, D. R. Stewart, C. N. Lau, R. S. Williams, *Nanotechnology* **2009**, *20*, 215201.
[47] P. Shewmon, *Diffusion in Solids*, 2nd ed., McGraw-Hill, New York, NY, USA **1963**.
[48] M. Noman, W. Jiang, P. A. Salvador, M. Skowronski, J. A. Bain, *Appl. Phys. A* **2011**, *102*, 877.
[49] Y. Ahn, S. Wook Ryu, J. Ho Lee, J. Woon Park, G. Hwan Kim, Y. Seok Kim, J. Heo, C. Seong Hwang, H. Joon Kim, *J. Appl. Phys.* **2012**, *112*, 104105.